Stanford Exploration Project, Report 79, November 16, 1997, pages 99–109

Stanford Exploration Project, Report 79, November 16, 1997, pages 99–109

3-D Hale-McClellan migration: A salt intrusion example

Gopal Palacharla and Biondo Biondi[1]

keywords: *algorithm, three-dimensional, velocity, imaging*

ABSTRACT

McClellan transformation offers a computationally efficient scheme for 3-D post-stack depth migration. The accuracy of the response of the McClellan filter is improved by rotating and averaging the filter. We have implemented the McClellan migration with the improved circular response and tested it on real data, a salt intrusion example. The migration collapses the diffractions, thereby delineating the salt and fault boundaries. The migration results obtained using different McClellan filters show only slight differences because of the limited dip and frequency range in the dataset we used for testing the algorithm.

INTRODUCTION

Two of the factors that determine the quality of a 3-D post-stack depth migration are the azimuthal isotropy of the impulse response of the algorithm, and the dip handling. Different techniques have been used to maximize the two factors as much as possible (Hale, 1991; Soubaras, 1992). McClellan transformation offers a computationally efficient scheme for depth extrapolation of 3-D seismic data in the frequency domain. The isotropy of the McClellan transformation depends on the accuracy of the approximation used for the "transformation" filter; this transformation filter is defined in the wavenumber domain $\vec{k}$ as $\cos \mid \vec{k} \mid$.

In our last report (Biondi and Palacharla, 1993) we suggested a method of improving the accuracy of the transformation filter, without increasing its computational cost. In SEP77 we have shown the impulse responses of the original and the improved filter, and have shown that the improved one has less dispersion than the original McClellan filter. Since the last report, we have further improved the circular response of the McClellan filter. This paper reports our use of a real dataset to study the the differences in the response of the different McClellan filters. The algorithm is implemented on the CM-5 in Fortran-90.

[1]**email:** not available

EXTRAPOLATION FILTERS

The explicit 3-D migration techniques consist of two stages. In the first stage, the filters for two-dimensional extrapolation are built and stored in a table. In the second stage the coefficients of the extrapolation filters are used along with the McClellan filters in the Chebyshev filter structure to extrapolate the wavefield in three dimensions.

We design our extrapolation filters for the migration using the following equation,

$$D(k) = \exp\left\{ i\frac{\Delta z}{\Delta x}\left[\sqrt{\left(\frac{\omega \Delta x}{v}^2\right) - k^2}\right]\right\} \tag{1}$$

and windowing techniques (Nautiyal et al., 1993; Parks and Burrus, 1987). We used a gaussian taper in the space domain. Although the filters are not optimized for a given dip and velocity model, they are designed to be stable. The McClellan extrapolation requires a look-up table of filters parametrized in terms of $\omega dx/v$. The filters are parametrized for $\omega dx/v$, so for a given $v(z)$ velocity model, the filters are designed for the range $\omega_{min} dx/v_{max}$ to $\omega_{max} dx/v_{min}$.

IMPROVED MCCLELLAN FILTERS

The McClellan filters proposed by Hale (1991) to approximate the cos $\mid \vec{k} \mid$ filter have the important advantage of being compact, and thus inexpensive to apply as convolutions in the space domain. The lower-order filter is applied by convolving the data with a nine-point stencil, the higher-order one by convolving the data with a 17-point stencil. However, both filters have an anisotropic impulse response, that is, their spectra vary with azimuth. Our last report (Biondi and Palacharla, 1993) suggested an improvement to the impulse response of the McClellan filter. The improved filter has less dispersion than either of the McClellan filters, and has a computational cost comparable to that of the 17-point filter. The new filter was obtained by averaging the 9-point McClellan filter with a 45 degree rotated version of it.

In this section we suggest a further improvement on the circular response of the McClellan filter. The representation of the 9-point McClellan filter in the wavenumber domain is:

$$\cos\sqrt{k_x^2 + k_y^2} \approx MC_0\left(k_x, k_y\right) = -1 + \frac{1}{2}\left(1 + \cos k_x\right)\left(1 + \cos k_y\right). \tag{2}$$

The modified McClellan transformation is given by the following equation from Hale (1991):

$$\cos\sqrt{k_x^2 + k_y^2} \approx -\frac{1}{2} + \frac{1}{2}(1 + \cos k_x)(1 + \cos k_y) - \frac{c}{2}(1 - \cos(2k_x))(1 - \cos(2k_y)) \tag{3}$$

where c is chosen by exactly matching a particular value k along the diagonal $k_x = k_y$. The value $c = 0.0255$ was used here, which corresponds to $k{=}\pi/3$.

Rotating the 9-point filter by an azimuth of 45 degrees and scaling the axes to match the original filter along the axes leads to the expression (Biondi and Palacharla, 1993):

$$\overline{MC_{45}}\left(\overline{k_x}, \overline{k_y}\right) = -1 + 2\left[\cos\left(\frac{\overline{k_x}}{2}\right) + \cos\left(\frac{\overline{k_y}}{2}\right) - 1\right]^2 . \tag{4}$$

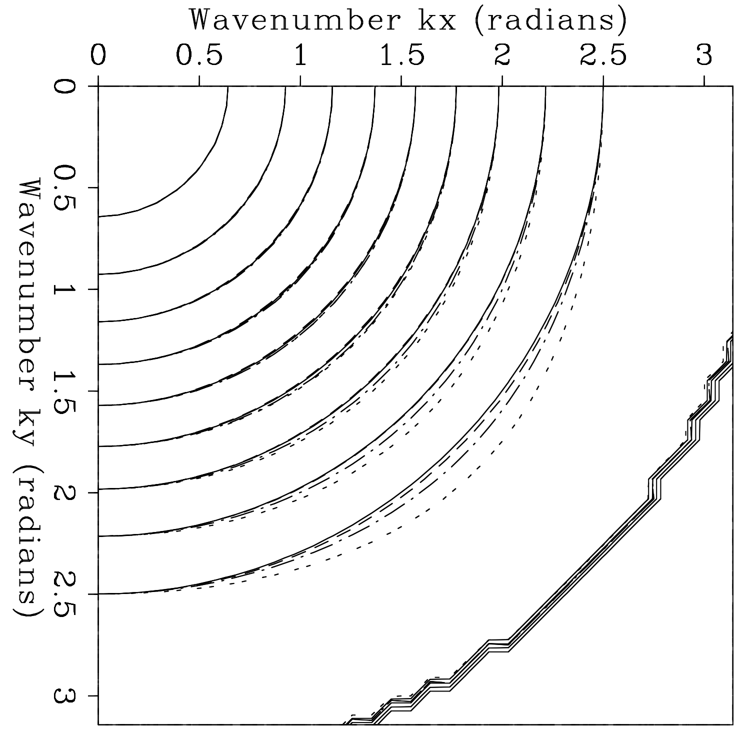

Figure 1: Contours of constant amplitude and phase for the 17-point McClellan transformation filter (double-dashed line), the 9-9 averaged filter (dot-dashed line), the 17-9 averaged filter (dashed line), and the ideal circularly symmetric filter (solid line). gopal1-all [ER]

The filter $\overline{MC_{45}}\left(\overline{k_x}, \overline{k_y}\right)$, as in equation (4) can be efficiently applied to the data because the operator $[\cos(k_x/2) + \cos(k_y/2) - 1)]$ is separable along x and y, its space-domain representation being a cross-shaped convolutional operator. The arms of the cross are the space-domain representation of the $cos(k/2)$ operator. In the last report, we got a more circular response by averaging (2), which represents the original nine-point filter with Equation (4) which represents the rotated 9-point filter. We call this filter the 9-9 averaged filter. Following similar reasoning as that leading to the nine-point averaged filter, the obvious thing to do would be to rotate the 17-point filter by 45 degrees azimuth and then average it with the original 17-point filter, after rescaling the axes such that the rotated 17-point filter matches the original one along the axes. However, it turns out that the remapping of the rotated 17-point filter leads to a fourth- degree equation, which is not simple to solve. Here we suggest, to average the 17-point McClellan filter as given by Equation (3) with the rotated 9-point filter as in Equation (4). We call this filter the 17-9 averaged filter. This new filter gives a more accurate result than the 9-9 averaged filter.

Figure 1 compares the spectrum of the 9-9 averaged filter (the dot-dashed line) with the ideal filter (the solid line) , the 17-point McClellan filter (the double-dashed line), and the 17-9 averaged filter(the dashed line). The spectra of the averaged filters are similar. Both exactly match the ideal spectrum along the axis and deviate from it considerably less than the spectrum of the 17-point McClellan filter across the whole range of azimuths. However, the 17-9 averaged filter gives the closest response to the ideal one. This filter could be realized in a similar way as the 9-9 averaged filter. By alternating the 17-point filter with the rotated 9-point filter on alternate depth steps.

DATA EXAMPLE

The impulse response tests of our algorithm, along with the comparisons with original 17-point McClellan filter have been shown in SEP77. Here we show the results on a real dataset described below. The migration code was run on the CM-5 at SEP.

The data are a 3-D dip-moveout corrected post-stack volume acquired over a salt intrusion in the Gulf of Mexico, donated by Halliburton Geophysical Services to SEP. The dataset is the same as that used by David Lumley (1993). The data used in testing the migration algorithm comprise a smaller portion of the complete dataset. We used a surface grid of 128x128 traces, with a decimated inline spacing of 50 meters and an original crossline spacing of 50 meters , representing a surface area of 6.4 km inline by 6.4 km crossline. The traces were further decimated to 8 milliseconds, since the data did not contain any signal beyond 60 Hertz. Since our present implementation of the migration algorithm requires the same spacing along the inline and crossline traces, the data along the inline directions were subsampled, giving a 50 meter spacing along the crossline. Figure 2 shows an inline section sliced at Y=4000 meters (20th slice) from the input stacked data volume. We migrated the data with a simple velocity function varying only with depth because SEP was given only the post-stack dataset and the available picked stacking velocities yielded an unreliable interval velocity model. Consequently we do not expect to properly focus reflections below the upper salt boundary, and possibly also the diffractions at the top of the salt are not perfectly focused.

We used a depth extrapolation step $dz = 10m$ and 300 depth steps for the migrations carried out using the different McClellan filters. The migrations were performed with the 9-point filter, the 17-point filter and the 9-9 averaged filter.

Figure 3 shows the inline slice taken from the migrated volume at the same position as the section in Figure 2. The diffractions seen in the input inline slice are now collapsed.

Figure 4 shows the crossline slices taken at X=10,800 meters. The slices are taken from the migrations performed using the nine-point filter (top) and the 9-9 averaged filter (bottom). The top of the salt can be seen at y=7000 meters and z=1380 meters.

Figure 5 shows the top of the salt body. The slices are taken from the migrations performed using the nine-point filter (top) and the 9-9 averaged filter (bottom), at z=1380 meters. The differences are small.

Figure 6 shows the depth slices taken at z=1600 meters from the migrations performed using the nine-point filter (top) and the 9-9 averaged filter (bottom). The differences are small. Figure 7 shows the difference of the sections shown in Figure 6. The peak amplitude in the difference section is 0.3 times of that in the original sections.

The lack of visible differences in the migrations performed by the 9-point and 9-9 averaged filters is most likely caused by the limited dip and frequency range in the dataset. Other causes can be an inaccurate velocity function that has prevented us from correctly imaging the diffraction at the top of the salt, and possibly the data size that reduced the migration aperture needed for imaging steeper dips.

CONCLUSIONS

We implemented a Hale-McClellan type migration algorithm for imaging 3-D post-stack data, with an option to vary the type of McClellan filter used in the migration. The migration does a good job of imaging the salt boundary and the faults by collapsing the diffractions caused by the salt sediment boundaries. Comparison of corresponding depth slices from data migrated using different McClellan transformation filters does not show large differences. The difference becomes clear, however, in a movie made of the depth slice alternating between the two McClellan filters. At this point, we have not been able to see the perceptible difference that we saw in the impulse response obtained using the rotated and original transformation filters, the results of which appear in our last report (SEP 77). The lack of visible differences is most likely caused by the limited dip and frequency range in the dataset. The other reasons can be an inaccurate velocity model and possibly insufficient migration aperture for imaging steep dips due to the data size. In the future we would like to test our migration algorithm on a dataset with a larger aperture and with more obvious steep dips.

ACKNOWLEDGEMENTS

Halliburton Geophysical Services kindly donated the data used in this paper. We would like to thank Mihai Popovici for converting the data to the seplib format and David Lumley for providing us with the velocity model he used for his imaging results.

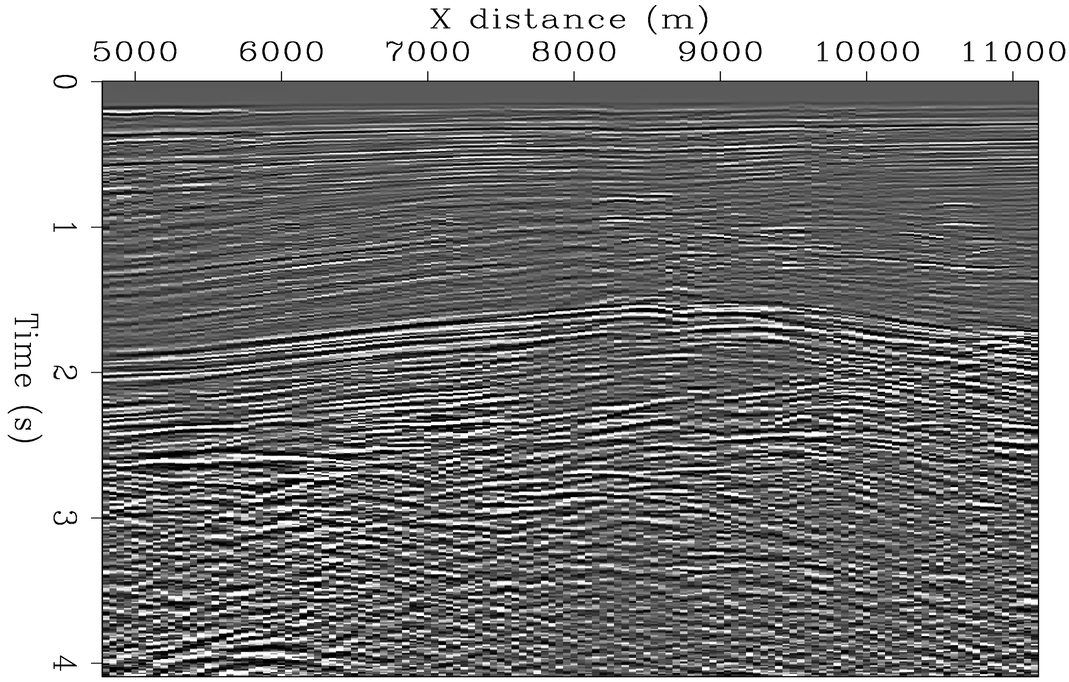

Figure 2: Inline section taken along crossline Y=4000 meters. The section shows much diffracted energy caused by salt-sediment interfaces. gopal1-inlint20 [ER]

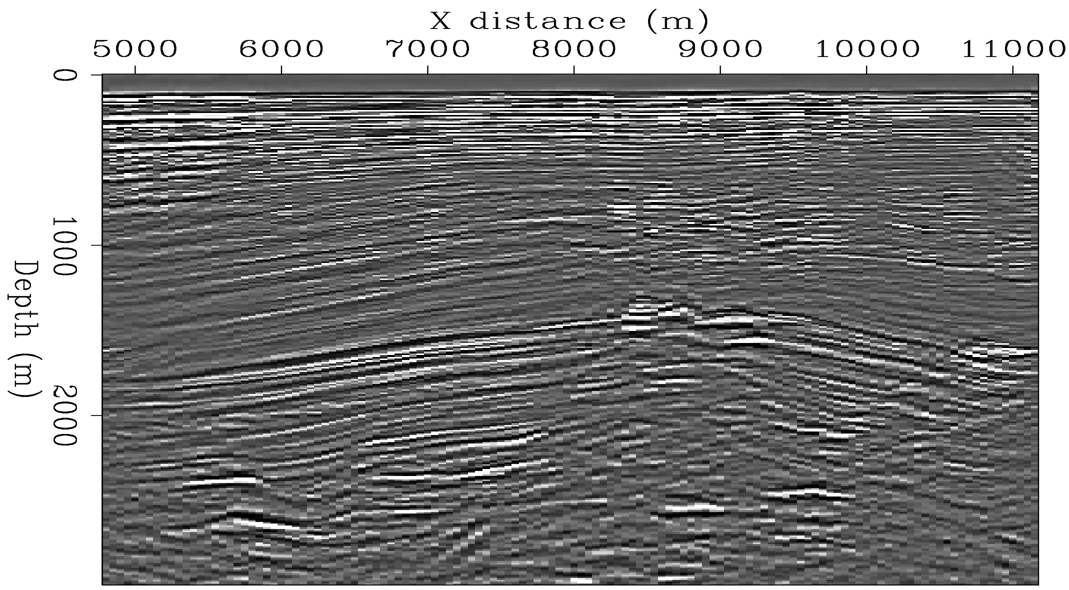

Figure 3: Inline section taken from the migrated volume at the same position as the section above in Figure 2. The 9-9 averaged filter was used in the migration. The diffractions are collapsed by the migration. The fault at (x=10,800 m) is clearly visible in the migrated section. gopal1-inlind620 [CR]

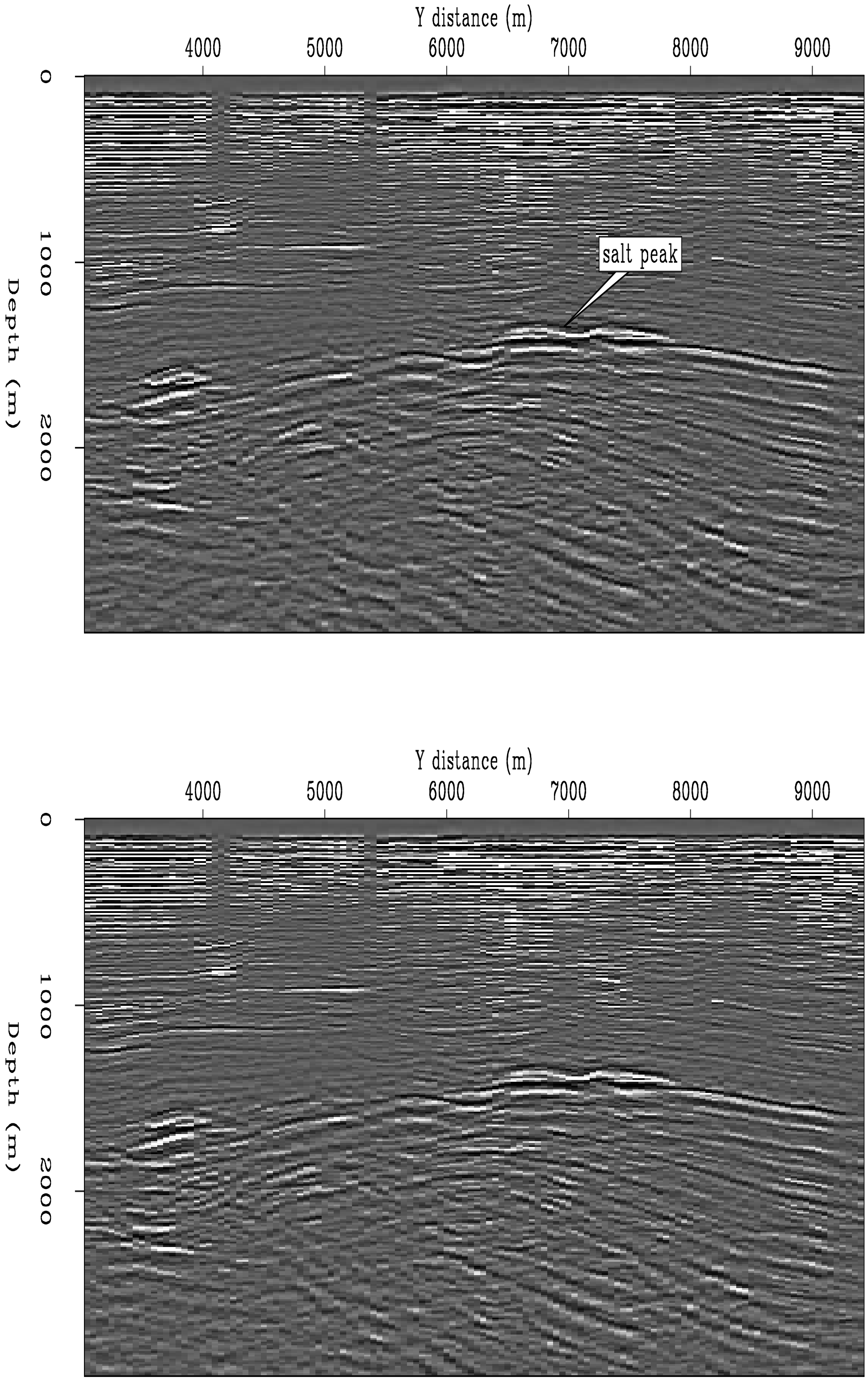

Figure 4: Cross slice taken along X=10800 meters. The top of the salt can be seen at Y=7000 meters and z=1380 meters. The top section shows the output of the nine-point filter and the bottom shows the output of the 9-9 averaged filter. Click button to see movie. gopal1-crsl117 [CR]

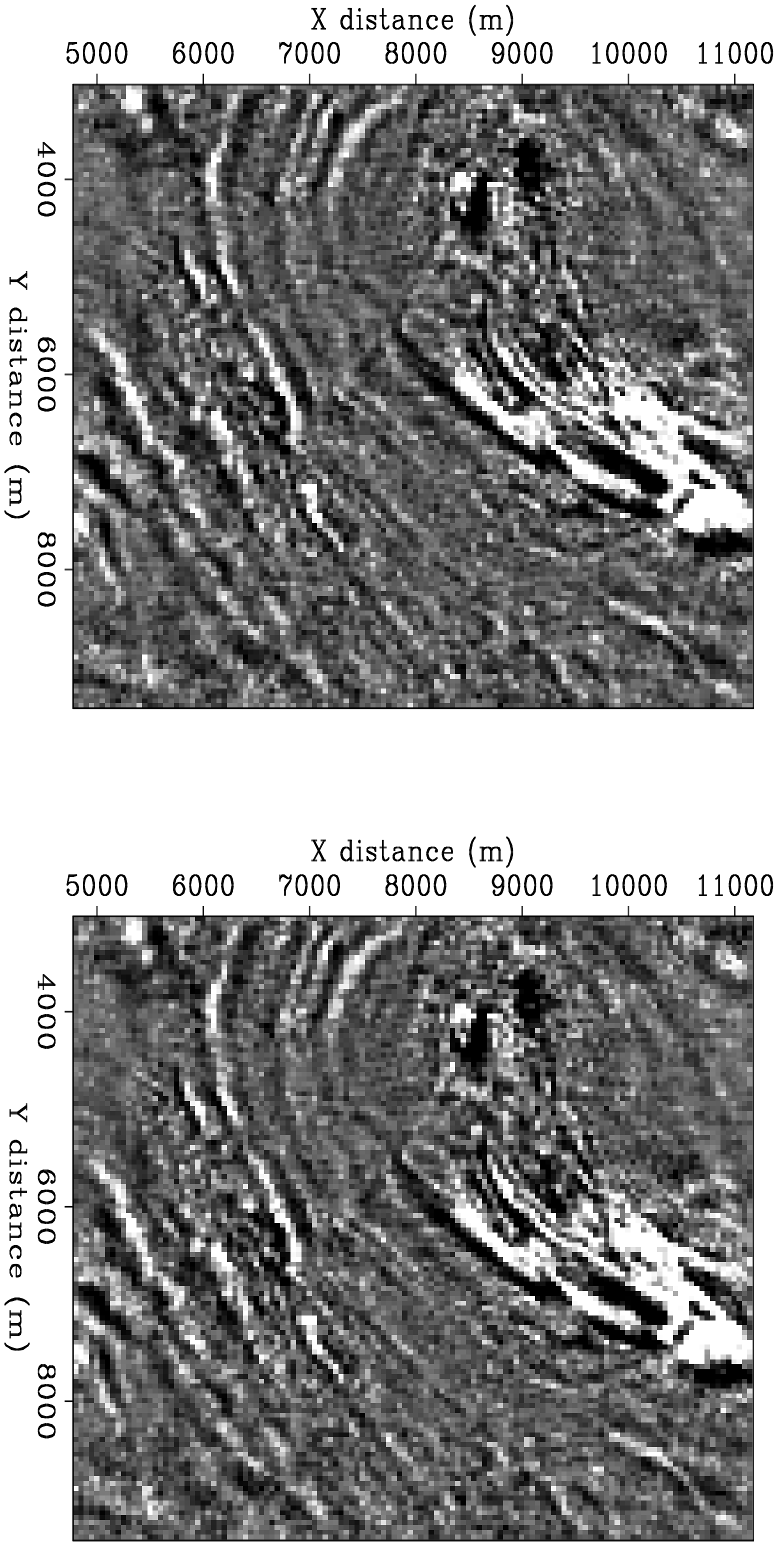

Figure 5: Top section, shows the depth slice at 1380 meters from the migration implemented using the nine-point filter, the bottom section is the corresponding one implemented using the 9-9 averaged filter. This depth slice shows the top of the salt. The differences between the two depth slices are small. Click button to see movie alternating between the two. gopal1-depsl138 [CR]

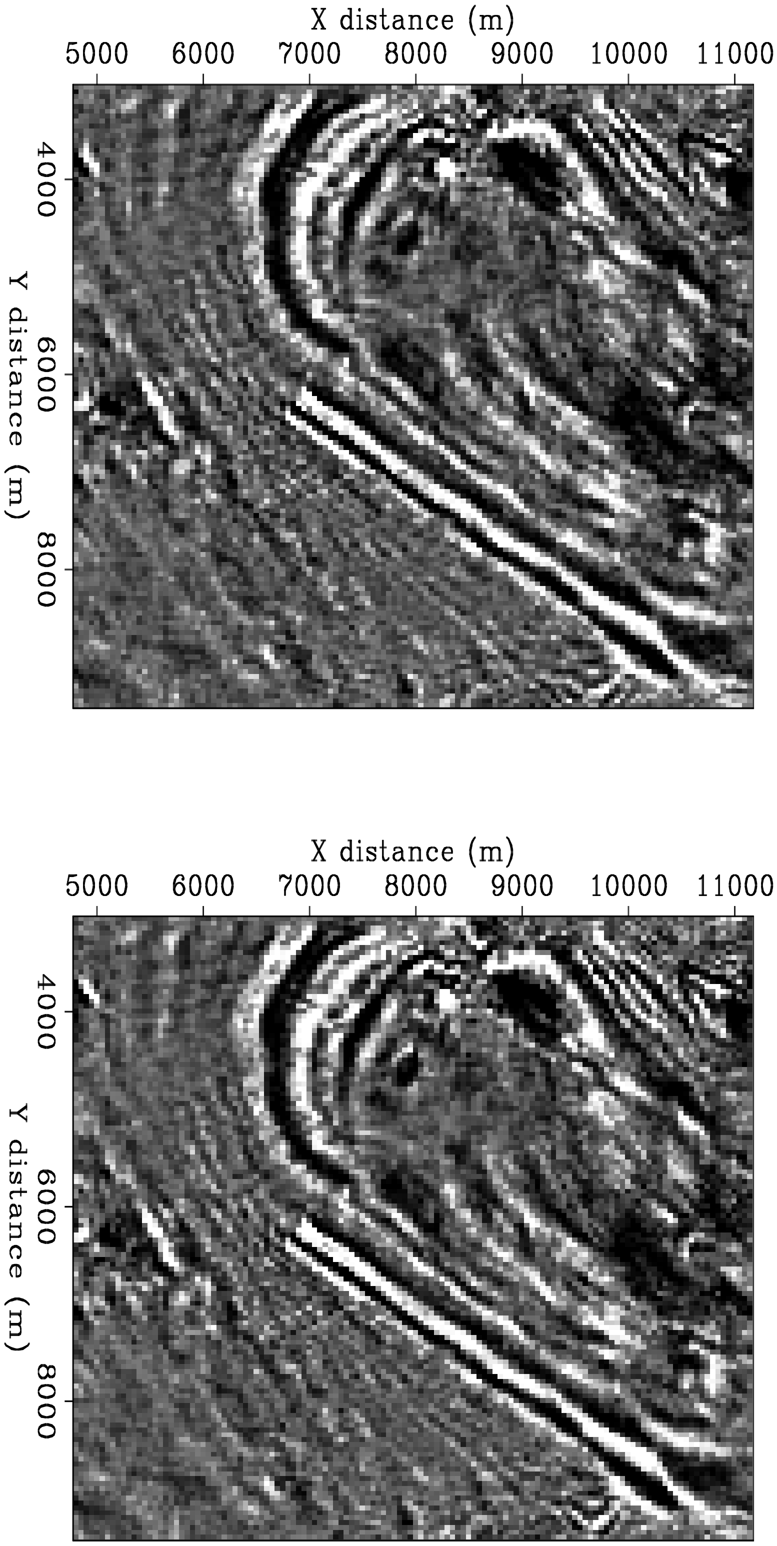

Figure 6: Depth slice at 1600 meters from the migration implemented using the nine-point filter (top), the same slice from the migration implemented with 9-9 averaged filter (bottom). The differences are small. The difference of the sections is shown in Figure 7. Click button to see a movie of the two slices. gopal1-depsl160 [CR]

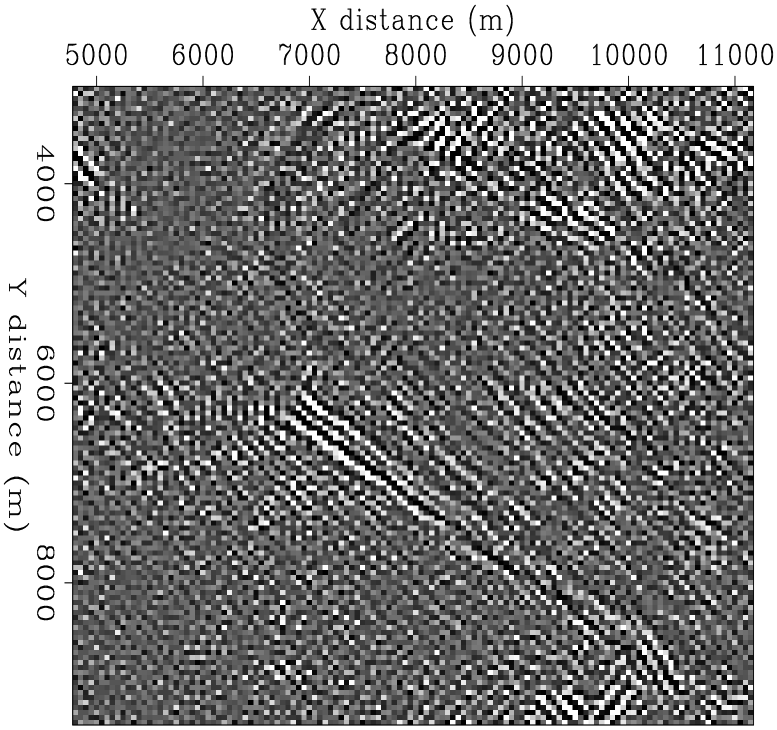

Figure 7: Difference in the depth slices shown in Figure 6. The peak amplitude is 0.3 times that of the peak amplitude in the depth slices. gopal1-diff160 [CR]

REFERENCES

Biondi, B., and Palacharla, G., 1993, 3-D wavefield depth extrapolation by rotated McClellan filters: SEP–**77**, 27–36.

Hale, D., 1991, 3-D depth migration via McClellan transformations: Geophysics, **56**, 1778–1785.

Lumley, D. E., 1993, Anti-aliased Kirchhoff 3-D migration: A salt intrusion example: SEP–**77**, 1–18.

Nautiyal, A., Gray, S. H., Whitmore, N. D., and Garing, J. D., 1993, Stability versus accuracy for an explicit wavefield extrapolation operator: Geophysics, **58**, 277–283.

Parks, T., and Burrus, C., 1987, Digital filter design: John Wiley and Sons.

Soubaras, R., 1992, Explicit 3-D migration using equiripple polynomial expansion and Laplacian synthesis: 62nd Ann. Internat. Mtg., Soc. Explor. Geophys., Expanded Abstracts, 905–908.